ISSN 1392-1207. MECHANIKA. Vol. 32, No. 3, 2026: 185–189

Sensitivity of Flutter Modelling Using the Non-Linear Vortex Lattice Method to Changes in Viscous Airfoil Data

Mindaugas DAGILIS*, Sigitas KILIKEVIČIUS**

**Kaunas University of Technology, Studentų g. 56-232, Kaunas, Lithuania, E-mail: mindaugas.dagilis@ktu.lt*

***Kaunas University of Technology, Studentų g. 56-232, Kaunas, Lithuania, E-mail: sigitas.kilikevicius@ktu.lt*

https://doi.org/10.5755/j02.mech.45273

1. Introduction

Low-fidelity aeroelasticity models are commonly used for various tasks where either high computational power is not available, or the task is highly iterative and even with high computational power available, the performance requirements of high-fidelity methods can be prohibitive [1-8]. The unsteady vortex lattice method is commonly used as the basis for low-fidelity aeroelastic modelling [4-8], having the advantage of being physics-based (no training or intermediate high-fidelity model data required) and more flexible in its implementation compared to the similar doublet lattice method.

While for most use cases, the regular unsteady vortex lattice method is sufficient, in highly aerodynamically non-linear cases the linear aerodynamic model can introduce high errors. For these cases, the non-linear unsteady vortex lattice method can be used. While this model has several variations [4, 6], a common one is the α-correction method [7, 8], which uses airfoil data determined either experimentally or using a viscous and/or compressible higher fidelity analysis to correct the output of the regular unsteady vortex lattice method.

While generally providing good results and reasonable computational performance, this method is dependent on the airfoil data, which is not always easily available. Both experimental and computational methods can introduce errors, reducing the quality of the model output. However, the effect that the variation in airfoil data quality has on the output of the non-linear unsteady vortex lattice method has not been analyzed in earlier research. This paper will attempt to quantify this influence and determine if variations in airfoil data quality are critical to the aeroelastic flutter prediction results, or if the method is sufficiently robust and not heavily influenced by the variations.

To achieve this, a flutter prediction analysis is performed for a cantilever mounted wing, changing the airfoil lift curve and comparing the results. The structural dynamics model and other parameters of the aerodynamic model are kept constant, to isolate the influence of the airfoil lift curve.

2. Methodology

The comparative flutter analysis is ran using a non-linear unsteady vortex lattice method coupled with Euler-Bernoulli beam structural dynamics. The aerodynamic and structural models are weakly coupled, exchanging information only once per time-step.

2.1. Aerodynamic model

The aerodynamic model used for the aeroelastic analysis is the non-linear unsteady vortex lattice method. The ring-vortex formulation is used, with a fully deformable wake and Rosenhead smoothing. Additionally, the α-correction is used to account for the non-linear lift curve of the airfoil.

The wing mesh is made up of 8 chord-wise and 16 span-wise elements, with a wake length of 10 elements. This number of elements is found to be sufficient for the analyzed case after a mesh-convergence analysis. Although the wing is based on a half-span cantilever mounted wind tunnel model, a full-span symmetric wing is modeled, mirrored around the ground plane. Mirroring the geometry is the standard method of modeling a ground plane in the vortex lattice method.

2.2. Structural dynamics model

The structural dynamics part of the aeroelasticity model is based on the Euler-Bernoulli beam element formulation for the stiffness and mass matrices. The generalized-α time discretization scheme [10] is used. The structural model is geometrically non-linear, with the stiffness, inertia and damping matrices updated iteratively during each time-step based on element rotations.

The structural properties of the model are based on a wind tunnel model described in [9]. The wing has a half-span of 0.324 m, and the derived beam properties of the wing are presented in Table 1, where X is the chordwise, Y the spanwise, and Z the normal direction. These structural properties were determined based on static structural tests and frequency response analysis of the wind tunnel model.

Table 1

Structural properties of the analyzed beam model

Parameter	Value
EA	4.20×10^{6} N
EI_{xx}	1.92×10^{-7} Nm^2
GI_{yy}	5.60×10^{-4} Nm^2
EI_{zz}	3.98×10^{-7} Nm^2
ρA	2.15×10^{-1} kg/m
ρI_{xx}	3.25×10^{-9} kgm
ρI_{yy}	3.27×10^{-5} kgm
ρI_{zz}	2.08×10^{-5} kgm

In addition to the main beam structure, three point masses were added to the model, representing the accelerometers, wingtip rod and extra weights. They were places 0.316 m, 0.330 m and 0.330 m from the wing root, with the masses equal to 0.0058 kg, 0.0070 kg and 0.0106 kg. For the accelerometers, the rotational inertia was neglected, while for the remaining two points masses it was set to 5.83×10^{-6} kgm^2 and 2.24×10^{-5} kgm^2 (with an equal inertia around *Y* and *Z* axes, the *X* inertia was set to zero).

2.3. Lift curves

The lift curves used for the non-linear correction are mathematically constructed, to make easy adjustments of the curve shape possible, using the following equations:

$$C_{L,1-2}(\alpha) = \alpha C_{L\alpha 1}, \tag{1}$$

$$C_{L,2-3}(\alpha) = \alpha C_{L\alpha 2} + C_{L,off2}, \tag{2}$$

$$C_{L,3-4}(\alpha) = \alpha C_{L_{max},w}\sqrt{1-\frac{(\alpha-\alpha_{cr})^2}{\alpha_{cr,w}^2}} + C_{L_{max}} - C_{L_{max},w}, \tag{3}$$

$$C_{L,4-5}(\alpha) = C_{L_{max},2}\sin 2\alpha. \tag{4}$$

Here, C_L is the lift coefficient with numeric indexes corresponding to ranges between points in Fig. 1, α is the angle of attack, $C_{L\alpha1}$ and $C_{L\alpha2}$ are the lift curve slopes for the two linear portions of the curve, $C_{L,off2}$ is the lift coefficient offset of the second linear portion, α_{cr} is the critical angle of attack, C_{Lmax} is the maximum lift coefficient before stall, $C_{Lmax,w}$ is the vertical semi-axis defining the rounded portion of the stall region (3-4 in Fig. 1), $\alpha_{cr,w}$ is the horizontal semi-axis defining the same rounded stall region, $C_{Lmax,2}$ is the maximum lift of the airfoil after stall.

Some of the parameters of the equations are freely chosen, while others are calculated in order to fulfil three constraints. The first one is that there must be no jump in the lift coefficient value at point 2 (in Fig. 1), the second and third are that there must be no jump in the value of both the lift coefficient curve and its first derivative at point 3. An additional optional constraint is introduced to link the values of $C_{Lmax,w}$ and $\alpha_{cr,w}$, in order to reduce the size of the analysed parameter space. The constraints are satisfied with the following equations:

$$\alpha_{cr,w} = 0.1745 C_{L_{max},w}, \tag{5}$$

$$\alpha_3 = -\frac{\alpha_{cr,w}^2}{\sqrt{\frac{C_{L_{max},w}^2}{C_{L\alpha 2}^2}+\alpha_{cr,w}^2}} + \alpha_{cr}, \tag{6}$$

$$C_{L,off2} = C_{L,3-4}(\alpha_3) - \alpha_3 C_{L\alpha 2}, \tag{7}$$

$$\alpha_2 = \frac{C_{L,off2}}{C_{L\alpha 1} - C_{L\alpha 2}} a. \tag{8}$$

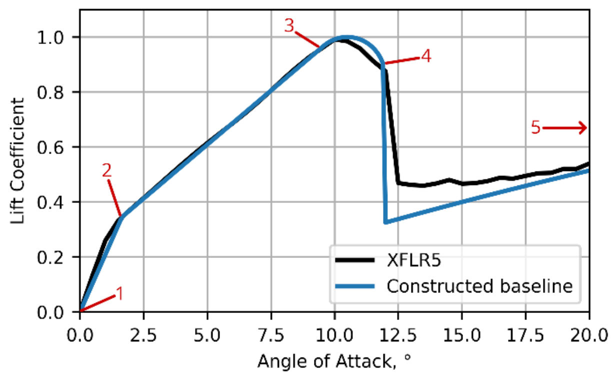

Fig. 1 NACA 0012 lift curve from an XFLR5 simulation and the mathematically constructed baseline curve

Table 2
The parameters of the baseline and modified lift curves

Parameter	Value for the baseline curve	Value for the modified curves	Percentage difference
$C_{L\alpha1}$	12.0	13.2	+10%
$C_{L\alpha2}$	4.5	4.95	+10%
C_{Lmax}	1.0	1.1	+10%
α_{cr}	10.5°	11.55	+10%
$C_{Lmax,w}$	0.15	0.3	+100%

The remaining five parameters $C_{L\alpha1}$, $C_{L\alpha2}$, C_{Lmax}, α_{cr} and $C_{Lmax,w}$ are freely chosen to define the lift curve. The curve used as the baseline is created based on the lift curve of the NACA 0012 airfoil generated using the XFLR5 software at 100 000 Re. While this curve might not be fully realistic and represents only a single operational point of a single airfoil, it is only used as the basis to make further changes, and follows a similar pattern to experimentally obtained curves for the same airfoil [11]. The comparison of the lift curve generated by XFLR5 and the mathematically constructed baseline curve is shown in Fig. 1. The parameter values used for the baseline lift curve are given in Table 2, together with the modified values that were used for the comparison curves. The curve shows a clear bi-linear shape, with a high lift slope at very low angles of attack, which then suddenly decreases and stays constant until stall. The transition from unstalled to fully stalled airfoil is quite sharp, but the peak of the curve is rounded.

As can be seen in Table 2, all of the parameters are increased by 10% to obtain the comparison curves. The only exception is $C_{Lmax,w}$, which is increased by 100% as it only has a relatively small influence on the curve shape compared to the other parameters. Only one parameter is changed for each modified curve in order to isolate their influence on the flutter results, providing 5 modified curves in total, which can be seen in Fig. 2.

Because of the additional constraints imposed on the curves, most of the parameter changes are not local, and have an influence on the overall curve shape. The only change that is completely local to the 1-2 region is the change in $C_{L\alpha1}$, whereas changing all other parameters has an influence on both the 2-3 and the 3-4 regions. A different mathematical curve formulation could allow changes which are more local while maintaining all the same constraints,

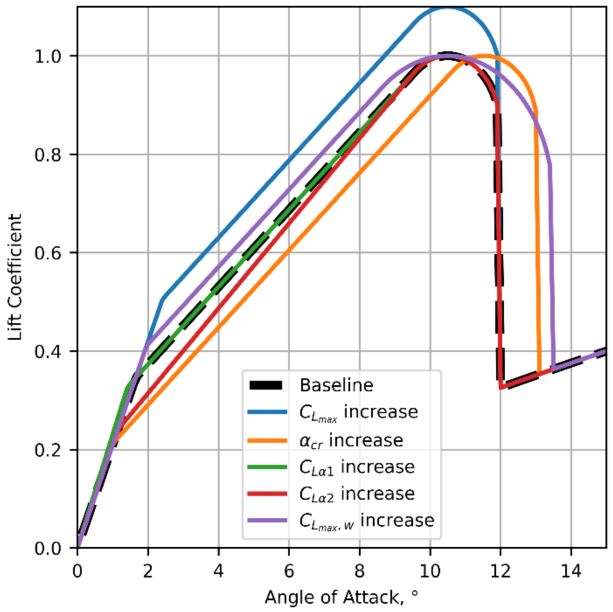

Fig. 2 Plot of the modified lift curves compared to the initial baseline lift curve

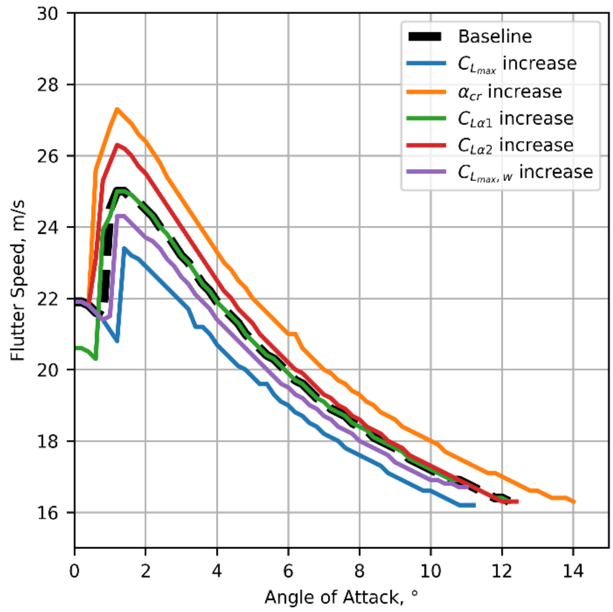

Fig. 3 Flutter speed change with angle of attack for the different lift curves (*Y*-axis doesn't begin at zero to make differences more visible)

but would likely reduce the available range of parameter values which yield a valid curve.

2.4. Determining the flutter speed

The flutter analysis for each lift curve is performed by running time-domain aeroelasticity modeling using the described model at angles of attack 0°-15°, at a step of 0.2°. At 0°, an initial guess for the flutter speed is provided, the model is run for 0.8 s (model time), and a frequency analysis of the results is performed for two windows to check if the oscillation amplitude is increasing or decreasing. If it is decreasing, the chosen speed exhibits no flutter, and the speed is increased in intervals of 0.1 m/s, re-running the model until flutter is found. If the amplitude is increasing, flutter is present at the tested speed, and the speed is decreased, until flutter is no longer observed. Each of these cases provide the flutter limit speed for that angle of attack, which is then recorded, the angle of attack is increased, and the same procedure is repeated to find the new flutter speed, using the previous one as the initial guess.

It is found that in the tested cases, after a certain angle of attack flutter is no longer observed. Because of this, the model is setup to stop if the speed is increased by 4 m/s from the previous flutter point and no new flutter limit is found.

3. Results and Discussion

The main result that is analyzed in this study is the change of flutter speed with angle of attack. This change for the different lift curves is shown in Fig. 3 and is compared to the baseline case in Fig. 4. All flutter speed curves follow the same general pattern, starting at a relatively low flutter speed of 20.6-21.9 m/s, which then suddenly increases to 23.4-27.3 m/s. This shift happens at 0.4°-1.2° angle of attack. After reaching this flutter peak, the flutter speed then starts decreasing, reaching a minimum of 16.2-16.7 m/s. The flutter stops completely at 11.0°-14.0° angle of attack.

The sudden increase in flutter speed that is seen in

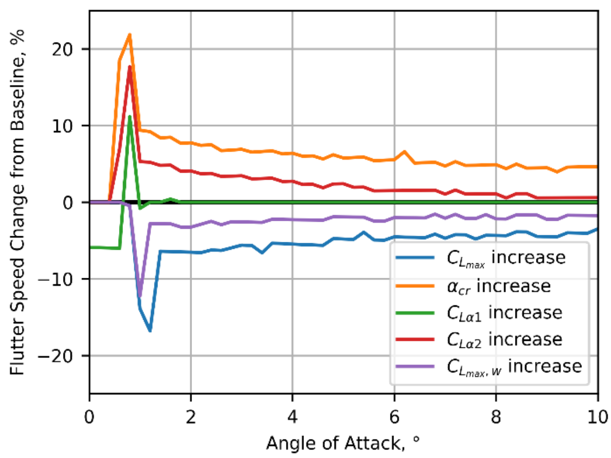

Fig. 4 Difference of flutter speed between the modified lift curves and the baseline lift curve

all cases is caused by the transition from region 1-2 to region 2-3 of the airfoil lift curve, and the change in airfoil lift slope. A higher lift slope increases the strength of the torsion-lift coupling that is the driving mechanism of flutter and subsequently causes it to happen at lower flow speeds. When this speed shift happens appears to be determined solely by the angle of attack at which the lift slope transition takes place, with the shift happening first in the two curves that have the earliest lift slope transition. However, the flutter speed shift always happens at a lower angle of attack than the lift slope transition, which is the opposite of what would be expected when switching from the 2D airfoil lift curve to the 3D flutter analysis, where the effective local angle of attack is lower than the geometric angle of attack. Intuitively, this should cause the speed increase to happen later in the 3D case, rather than earlier. A likely explanation is that as the angle of attack oscillates during the flutter cycle, it enters the 2-3 region of the lift curve, even though the average angle of attack is lower.

As expected, the initial flutter speed at 0° is governed by the lift slope of the first linear section, and decreases when this lift slope is increased. The 10% increase in the lift slope has caused a 5.9% reduction of the flutter speed. Looking at Fig. 4, it appears that the increased lift slope in region 1-2 has at least some influence up to 1.6° angle of attack, which is where the change to region 2-3 happens.

It is more difficult to isolate the influence of the other lift curve modifications. Mostly the influence appears to be related to the increase or decrease of lift in region 2-3, with the two cases that have an increased lift showing a decrease in flutter speed, and the two cases with decreased lift have an increase in flutter speed. In this case the effect is most likely not related directly to aerodynamics, but to the non-linear structural dynamics model. With a higher lift coefficient, the structure is deformed more due to the higher steady aerodynamic forces. For an unswept wing geometry such as this one, the deformation creates a coupling between the torsion and in-plane bending modes, reducing their frequencies. In the specific case of this wing, this brings the torsion mode frequency closer to the second out-of-plane bending mode, causing them to couple more easily, and achieve flutter.

The lift of the wing appears to be more important than the lift slope in the 2-3 region, because the test case with the increased $C_{L\alpha 2}$ shows a larger difference from baseline at lower angles of attack (where the lift is more different), and this difference decreases as the lift difference decreases at higher angles of attack. The difference in the lift slopes is constant, suggesting that it is not the cause of this decreasing flutter speed difference. The other cases, where the difference of lift from the baseline is constant in the 2-3 region also show this reduction in difference at higher angles of attack, but the reduction is much more pronounced in the increased $C_{L\alpha 2}$ case, decreasing from +5.3% to just +0.5%, whereas for the three other cases the decreases are from +9.5% to +4.7%, from −2.8% to −1.8%, and from −6.3% to −3.4%.

At the transition between regions 1-2 and 2-3, very high difference spikes are seen in Fig. 4. This is less indicative of actual difference in lift coefficient values, and more indicative of the difference of when the shift to a lower lift slope happens. For the cases where the transition happens earlier, a positive spike is seen, because their flutter speed suddenly increases before the shift happens for the baseline curve. For the cases where the transition is delayed, a negative spike is seen instead. The spikes range from −16.6% to +21.8%.

If the spikes are ignored, the difference stays within ±10% for all the analyzed lift curves. The largest difference is seen for the α_{cr} increase case, reaching +9.3% just after the difference spike. The largest negative difference is in the C_{Lmax} increase case, reaching −6.3%. In most cases, these results would be acceptable for a flutter analysis, especially for one conducted using relatively low-fidelity methods. The smallest difference is seen for the $C_{Lmax,w}$ increase case, even though the parameter itself had the largest increase.

When comparing the change of maximum angle of attack where flutter happens, we can see that an increased α_{cr} and $C_{L\alpha 2}$ increases this angle of attack, and an increased C_{Lmax} and $C_{Lmax,w}$ decrease it. The baseline angle is 12.2°. In general, the flutter stops because of the decreased (or reversed) lift slope around the stall angle. The change in $C_{L\alpha 2}$ has a small effect, only increasing it by 0.2°, likely directly because of the increased lift slope making flutter happen easier. The change in α_{cr} increases the angle by 1.8°, having the strongest overall effect. This change is intuitive, as the increase in α_{cr} delays the reduction of lift slope caused by stall. Increased C_{Lmax} decreases the angle by 1.0°, this change is not as easily explainable, because as mentioned earlier the increased lift shifts decreases the torsion frequency of the wing and usually makes the flutter happen easier. It could be caused by the increased lift also increasing wing twist, effectively increasing the angle of attack at the tips and causing them to stall earlier. The increased $C_{Lmax,w}$ decreases the angle by 1.2°, this change happens because of the decreased lift slope in a wider region around stall.

Overall, the flutter prediction appears to be most sensitive to changes in α_{cr} and C_{Lmax}, whereas lift slope differences appear to be most important at low angles of attack. Changes in the shape of the curve near stall appears to have the smallest effect, even though the modified corresponding parameter was changed much more than the other analyzed parameters of the lift curve.

The results show that variations in the airfoil lift curve used for the non-linear corrections of unsteady vortex lattice method have a noticeable, but not critical effect on flutter prediction. For any parameter of the curve changed by 10%, the corresponding change of flutter speed at any angle of attack was within the ±10%, if the localized spikes caused by the shift in the lift slope transition are ignored. This result shows that the modeling framework is quite robust, and even considerable variations in the airfoil lift slope still give flutter prediction results which would be considered acceptable for low fidelity models.

4. Conclusions

In the study, the effect that variations in the airfoil lift curve have on flutter prediction using the non-linear unsteady vortex lattice method was analyzed. From the results, the following conclusions can be made:

1. The unstalled portion of an airfoil lift curve can be sufficiently accurately described by mathematical equations, allowing parametrization and easy modification of the curve shape.

2. At low angles of attack, the flutter prediction results are somewhat sensitive to the local lift slope, with a 10% lift slope increase causing a 6.8% flutter speed decrease. At higher angles of attack, it's more difficult to isolate this effect from the difference in lift, but it appears that near stall and at similar lift values, a 10% lift slope increase only causes a 0.5% flutter speed increase.

3. Changes of lift appear to play a bigger role than lift slope at higher angles of attack, with 3 curves that have the same lift slope but different lift values showing differences from baseline in the −6.3% to +9.3% range.

4. Overall changing any of the analyzed lift curve parameters by 10% appears to cause a change in flutter speed that is within ±10% compared to the baseline, showing the sufficient robustness of the method against airfoil lift data uncertainty.

References

1. **Li, S.; Caracoglia, L.; Møller-Madsen, J.** 2023. Examining adequacy of the empirical Theodorsen function for wind turbine blade section-model aeroelasticity, Journal of Fluids and Structures 118: 103843. https://doi.org/10.1016/j.jfluidstructs.2023.103843.
2. **Das, A.; Marzocca, P.; Coppotelli, G.; Levinski, O.; Taylor, P.** 2024. A data-driven approach for rapid detection of aeroelastic modes from flutter flight test based on limited sensor measurements, Mechanical Systems and Signal Processing 220: 111712. https://doi.org/10.1016/j.ymssp.2024.111712.
3. **Gulizzi, V.; Benedetti, I.** 2024. Computational aeroelastic analysis of wings based on the structural discontinuous Galerkin and aerodynamic vortex lattice methods, Aerospace Science and Technology 144: 108808. https://doi.org/10.1016/j.ast.2023.108808.
4. **Campagna, D.; Gulizzi, V.; Benedetti, I.** 2025. A DG-VLM framework for computational static aeroelastic analysis of composite wings, Composite Structures 353: 118697. https://doi.org/10.1016/j.compstruct.2024.118697.
5. **Dagilis, M.; Lendraitis, M.; Kilikevičius, S.** 2025. Feasibility of Real-time Aeroelasticity Modeling Using the Unsteady Vortex Lattice Method, AIAA Aviation Forum and ASCEND 2025: 3844. https://doi.org/10.2514/6.2025-3844.
6. **Epps, B.P.; Roesler, B.T.; Medvitz, R.B.; Choo, Y.; McEntee, J.** 2019. A viscous vortex lattice method for analysis of cross-flow propellers and turbines, Renewable Energy 143: 1035-1052. https://doi.org/10.1016/j.renene.2019.05.053.
7. **Parenteau, M.; Laurendeau, E.** 2021. A transonic, viscous nonlinear frequency domain Vortex Lattice Method for aeroelastic analyses, Journal of Fluids and Structures 107: 103406. https://doi.org/10.1016/j.jfluidstructs.2021.103406.
8. **Parenteau, M.; Laurendeau, E.** 2020. A general modal frequency-domain vortex lattice method for aeroelastic analyses, Journal of Fluids and Structures 99: 103146. https://doi.org/10.1016/j.jfluidstructs.2020.103146
9. **Dagilis, M.; Lendraitis, M.; Kilikevičius, S.** 2026. Low Reynolds Number Wind Tunnel Aeroelastic Analysis of a Low-Stiffness Wing at High Angles of Attack, International Forum on Aeroelasticity and Structural Dynamics 2026: 0260.
10. **Hulbert, G.M.; Chung, J.** 1996. Explicit time integration algorithms for structural dynamics with optimal numerical dissipation, Computer Methods in Applied Mechanics and Engineering 137(2): 175-188. https://doi.org/10.1016/S0045-7825(96)01036-5.
11. **Jardin, T.; Ferrand, V.; Gowree, E.R.** 2025. NACA0012 airfoil at Reynolds numbers between 50,000 and 140,000 — Part 1: Steady freestream, International Journal of Heat and Fluid Flow 112: 109655. https://doi.org/10.1016/j.ijheatfluidflow.2024.109655.

M. Dagilis, S. Kilikevičius

SENSITIVITY OF FLUTTER MODELLING USING THE NON-LINEAR VORTEX LATTICE METHOD TO CHANGES IN VISCOUS AIRFOIL DATA

S u m m a r y

This paper presents an analysis of how sensitive non-linear vortex lattice method based aeroelasticity models are to variations in viscous airfoil data. These models are a useful low-fidelity tool for fast aeroelastic analysis, often used in early aeroelastic aircraft design and flight control law development. However, they are reliant on pre-existing availability of viscous airfoil data, which can be difficult to obtain without expensive wind tunnel testing or high-fidelity CFD computations. To determine how sensitive the aeroelastic results are to the variations in this airfoil data, a flutter simulation is run for the same wing test case, but using several different airfoil performance curves. The results are analyzed to determine how much influence on the final flutter results these changes have. It is found that when modifying various parameters of the lift curves by 10%, in most of the angle of attack range the differences from baseline stay within ±10%.

Keywords: non-linear aeroelasticity, vortex lattice method, computational aerodynamics.

Received June 11, 2026
Accepted June 19, 2026